

# Single-photon nonlinearities in a strongly driven optomechanical system with quadratic coupling

Hong Xie,<sup>1,2,3</sup> Gong-Wei Lin,<sup>4</sup> Xiang Chen,<sup>1,2</sup> Zhi-Hua Chen,<sup>1,2</sup> and Xiu-Min Lin<sup>1,2,\*</sup>

<sup>1</sup>Fujian Provincial Key Laboratory of Quantum Manipulation and New Energy Materials, College of Physics and Energy, Fujian Normal University, Fuzhou 350117, China

<sup>2</sup>Fujian Provincial Collaborative Innovation Center for Optoelectronic Semiconductors and Efficient Devices, Xiamen 361005, China

<sup>3</sup>College of JinShan, Fujian Agriculture and Forestry University, Fuzhou 350002, China

<sup>4</sup>Department of Physics, East China University of Science and Technology, Shanghai 200237, China

(Received 7 April 2016; published 29 June 2016)

Optical nonlinearities at the single-photon level are explored in a quadratically coupled optomechanical system, where the cavity frequency is coupled to the square of the mechanical displacement. The effective nonlinear interaction between photons and phonons is enhanced by a strong driving field, which allows one to implement the single-photon nonlinearities even if the single-photon coupling strength  $g_0$  is much lower than the cavity decay rate  $\kappa$ . The photon statistical properties are discussed by calculating the second-order correlation function both analytically and numerically. The results show that the single-photon nonlinearities are robust against mechanical thermal noise in the strong-coupling and sideband-resolved regime, and photon blockade and photon-induced tunneling can be realized with experimentally accessible parameters.

DOI: [10.1103/PhysRevA.93.063860](https://doi.org/10.1103/PhysRevA.93.063860)

## I. INTRODUCTION

Realization of single-photon nonlinearities is a central topic in quantum optics. In the past few decades, strong optical nonlinearities at the single-photon level have been intensively studied in cavity QED [1,2], quantum dots [3], and Rydberg atomic systems [4,5], with practical relevance for quantum computation and quantum information. Recently, a lot of attention has been paid to optomechanical systems [6,7], where light is coupled to mechanical motion via radiation pressure. The optomechanical interaction between photons and phonons is nonlinear, which has been theoretically exploited to generate nonclassical state [8,9], to realize strong photon correlations [10–22], nondemolition measurement [23–25], etc. However, the nonlinear quantum optomechanics requires the single-photon coupling strength to exceed the cavity decay rate, namely,  $g_0 > \kappa$ . In spite of recent significant laboratory advances, this regime still presents daunting experimental challenges.

The simplest way to enhance the optomechanical coupling is to coherently drive the cavity, leading the coupling strength to gain a factor  $\sqrt{n}$ , where  $n$  is the average intracavity photon number. This approach has led to a number of interesting phenomena, for example, ground-state cooling [26–32], normal-mode splitting [33,34], optomechanically induced transparency [35–37], mechanically mediated state transfer [38–43], and the realization of squeezed light [44–46]. However, this enhancement comes at the cost of losing the intrinsic nonlinearity of the optomechanical coupling, namely, the interaction between photons and phonons is effectively linearized.

Recently, the enhancement of  $g_0/\kappa$  has been theoretically studied by using the Josephson effect in superconduction circuits [47], collective interactions in optomechanical arrays [48,49], and diamagnetic and demagnetizing effects in superconducting quantum magnetomechanics [50]. Remark-

ably, strong optical nonlinearities can also be realized in the weak-coupling case. For example, strong Kerr nonlinearities are induced by quantum criticality in a hybrid electro-optomechanical system [51], and single-photon nonlinearities are obtained by driving near optomechanical instability in a two-mode system [52] and by enhanced nonlinear coupling between the squeezed cavity mode and the mechanical mode [22].

Here, we study single-photon nonlinearities in a quadratically coupled optomechanical system [53–58]. Optomechanical quadratic coupling, where the cavity frequency is coupled to the square of the mechanical displacement, enables nonlinear interactions between photons and phonons [59–62] even when the optomechanical system is strongly driven. By driving the cavity on red two-phonon resonance, light-enhanced nonlinear coupling between photons and phonons results in an anharmonic energy-level diagram. Analogously to the Jaynes-Cummings ladder of the atom-cavity system [2,63,64], the anharmonic energy level provides a crucial feature to realize single-photon nonlinearities. To characterize photon statistical properties of the quadratically coupled system, the equal-time second-order correlation function is discussed both analytically and numerically. We find that photon blockade and photon-induced tunneling can be observed under the strong-coupling condition, i.e., the effective coupling strength  $g$  exceeds the cavity decay rate  $\kappa$ . This result is different from a previous study [58] where the stringent single-photon strong-coupling condition ( $g_0 > \kappa$ ) must be satisfied to realize photon blockade. Fortunately, in the strong-driving case, the effective coupling strength  $g = g_0\alpha$  can be enhanced and tuned by adjusting the amplitude of the driving field, which will reduce the experimental difficulty and extend its utility. Combined with the recent large enhancement of  $g_0$  in the photon crystal optomechanical cavity [65], the strong-coupling condition  $g > \kappa$  can be achieved in state-of-the-art experiments.

This paper is organized as follows. In Sec. II, we describe the theoretical model of a strongly driven optomechanical system with quadratic coupling and show that the nonlinear interaction between photons and phonons can be employed

\*xmlin@fjnu.edu.cn

to realize strong optical nonlinearities. Section III presents approximately analytical solutions and numerical results of the second-order correlation function in the few-photon subspace. Finally, we provide a brief outlook on the experimental feasibility of a strong-coupling and sideband-resolved regime and summarize the results in Sec. IV.

## II. THEORETICAL MODEL

The interaction between light and mechanics in a cavity optomechanical system is often termed dispersive, where the frequency of the cavity is dependent on the position of the mechanics oscillator,  $\omega(x) = \omega_c + \omega'x + \omega''x^2/2 + \dots$ . Here,  $\omega_c$  is the bare resonance frequency of the cavity,  $x = x_{\text{ZPF}}(b + b^\dagger)$  denotes the position of the mechanical oscillator with the zero-point fluctuation amplitude  $x_{\text{ZPF}}$ , and  $b$  expresses the annihilation operator of the mechanical mode. Consider a membrane-in-the-middle configuration [54,55], in which a thin dielectric membrane is placed inside a Fabry-Perot cavity, as shown in Fig. 1(a). When the membrane is located in the node (or antinode) of the cavity field, the first derivative of  $\omega(x)$  vanishes, i.e.,  $\omega' = 0$ , so that  $\omega''/2$  becomes the

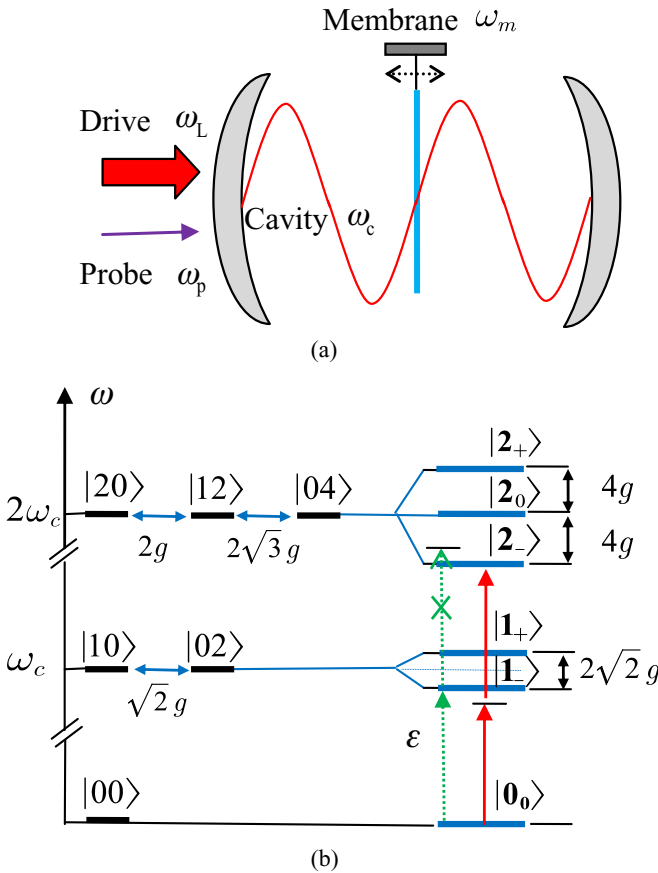


FIG. 1. (a) Schematic of a strongly driven optomechanical system with quadratic coupling. (b) Anharmonic level diagram for the relevant zero-photon, one-photon, and two-photon states. States are labeled  $|nm\rangle$ , where  $n$  ( $m$ ) denotes the photon (phonon) number. The effective coupling  $g$  splits the degeneracy between state  $|nm\rangle$  and state  $|n-1,m+2\rangle$ . Dotted green arrows describe the one-photon transition; solid red arrows, the two-photon transition.

dominant term for the optomechanical coupling. Thus we have  $\omega(x)a^\dagger a \simeq (\omega_c + \omega''x^2/2)a^\dagger a$ . After switching to the rotating picture at driving frequency  $\omega_L$ , the Hamiltonian of the quadratically coupled system reads

$$H_1 = [\delta_c + g_0(b + b^\dagger)^2](a^\dagger a - \langle a^\dagger a \rangle) + \omega_m b^\dagger b + H_{\text{dr}}, \quad (1)$$

where  $\delta_c = \omega_c - \omega_L$  is the detuning between the cavity and the driving fields,  $\omega_m$  denotes the mechanical frequency, and  $g_0 = \frac{1}{2}\omega''x_{\text{ZPF}}^2$  represents the single-photon quadratic coupling strength. Following previous studies [26,59], we have subtracted the steady-state average photon number  $\langle a^\dagger a \rangle$ , which renormalizes the mechanical frequency.  $H_{\text{dr}} = \Omega(a^\dagger + a)$  describes the driving term in the rotating picture, where the amplitude  $\Omega$  is related to the input laser power  $P_{\text{in}}$  and cavity decay rate  $\kappa$  by  $|\Omega| = \sqrt{P_{\text{in}}\kappa/\hbar\omega_L}$ .

For a sufficiently strong driving field, the cavity and mechanical modes can be split into an average coherent amplitude and a fluctuation term, i.e.,  $a \rightarrow \alpha + a$  and  $b \rightarrow \beta + b$ . Following the standard linearization procedure, one has the average coherent amplitudes

$$\dot{\alpha} = -\left(i\delta_c + \frac{\kappa}{2}\right)\alpha - ig_0\alpha(\beta + \beta^*)^2 - i\Omega, \quad (2a)$$

$$\dot{\beta} = -\left(i\omega_m + \frac{\gamma}{2}\right)\beta - i2g_0(|\alpha|^2 - \langle a^\dagger a \rangle)(\beta + \beta^*), \quad (2b)$$

where  $\gamma$  is the mechanical decay rate. In the steady-state case, one gains  $\alpha = \Omega/(-\delta_c + i\kappa/2)$  and  $\beta = 0$ , where the amplitude  $\alpha$  can be chosen real without loss of generality.

Then the driven-displaced Hamiltonian becomes

$$H_2 = \delta_c a^\dagger a + \omega_m b^\dagger b + g(a^\dagger + a)(b + b^\dagger)^2 + g_0 a^\dagger a(b + b^\dagger)^2 \quad (3)$$

with the effective coupling strength  $g = g_0\alpha$ . For the parameters [55]  $P_{\text{in}} = 5 \mu\text{W}$ ,  $\lambda = 1064 \text{ nm}$ ,  $\omega_m = 10^6 \text{ Hz}$ , and  $\kappa = 10^5 \text{ Hz}$ , one has  $\alpha \sim 10^4$ . Since  $g_0 \ll g$ , the second-order term  $g_0 a^\dagger a(b + b^\dagger)^2$  can be neglected. This is known as the linearization approximation. Under the conditions  $\delta_c = 2\omega_m$  and  $\omega_m \gg g$ , the rapidly oscillating terms with high frequencies  $\pm(\delta_c + 2\omega_m)$  and  $\pm\delta_c$  can be safely neglected under the rotating-wave approximation. Consequently, the effective Hamiltonian of the system can be written as

$$H_{\text{eff}} = \delta_c a^\dagger a + \omega_m b^\dagger b + g(a^\dagger b^2 + ab^\dagger)^2. \quad (4)$$

The validity of the effective Hamiltonian  $H_{\text{eff}}$  is numerically checked in the next section. Note that the nonlinear coupling  $g = g_0\alpha$  between the cavity and the mechanical modes can be enhanced and tuned by adjusting the amplitude of the driving field.

The nonlinear interaction in  $H_{\text{eff}}$  describes the process that the creation (annihilation) of a photon is accompanied by the annihilation (creation) of two phonons, which leads to a resonant interaction between state  $|n,m\rangle$  and state  $|n-1,m+2\rangle$ , where  $n$  ( $m$ ) represents the occupation number of the cavity (mechanical) mode. Because of its dependence on the photon number  $n$  and phonon number  $m$ , the corresponding coupling amplitude  $g\sqrt{n(m+1)(m+2)}$  will give rise to an

anharmonic level diagram, analogous to the Jaynes-Cummings ladder of the atom-cavity system.

Assume that only the lower energy levels of the cavity field and mechanical resonator are occupied, the effective Hamiltonian  $H_{\text{eff}}$  can be diagonalized in the few-photon subspace, resulting in dressed states as shown in Fig. 1(b). The eigenstates and eigenvalues of the system in the diagonal bases are denoted  $|0_0\rangle = |00\rangle$  and 0 in the zero-photon subspace,  $|1_{\pm}\rangle = \frac{1}{\sqrt{2}}(|10\rangle \pm |02\rangle)$  and  $\pm\sqrt{2}g$  in the one-photon subspace, and  $|2_{\pm}\rangle = \frac{1}{2\sqrt{2}}(|20\rangle \pm 2|12\rangle + \sqrt{3}|04\rangle)$ ,  $|2_0\rangle = \frac{1}{2}(-\sqrt{3}|20\rangle + |04\rangle)$ , and  $\pm 4g, 0$  in the two-photon subspace, respectively.

To exploit the light-enhanced nonlinear quadratic coupling, a weak field with frequency  $\omega_p$  and amplitude  $\varepsilon$  is used to probe the cavity mode [18,22]. In the rotating frame with  $\omega_L$ , the Hamiltonian of the probe field is  $H_p = \varepsilon(ae^{i\delta_p t} + a^\dagger e^{-i\delta_p t})$ , where  $\delta_p = \omega_p - \omega_L$ . In the rotating frame corresponding to the unitary operator  $U = e^{i(a^\dagger a + b^\dagger b)/2\delta_p t}$ , the Hamiltonian  $H_{\text{eff}} + H_p$  including the probe field is given by

$$\tilde{H}_{\text{eff}} = \Delta d^\dagger d + \tilde{\omega}_m b^\dagger b + g(a^\dagger b^2 + ab^\dagger)^2 + \varepsilon(a + a^\dagger), \quad (5)$$

where  $\Delta = \delta_c - \delta_p = \omega_c - \omega_p$  describes the detuning between the cavity mode and the probe field, and  $\tilde{\omega}_m = \omega_m - \delta_p/2 = \Delta/2$  satisfies the two-phonon resonant condition in this new rotating frame.

### III. PHOTON BLOCKADE AND PHOTON TUNNELING

To characterize the photon statistical properties of the cavity field, we study the average intracavity photon number  $\langle n \rangle = \langle a^\dagger a \rangle$  and equal-time second-order correlation function  $g^{(2)}(0) = \langle a^\dagger a^2 \rangle / \langle a^\dagger a \rangle^2$ . The condition  $g^{(2)}(0) < 1$  corresponds to sub-Poisson statistics of the cavity field, which is a nonclassical effect often referred to as photon antibunching, and the limit  $g^{(2)}(0) \rightarrow 0$  indicates complete photon blockade, in which two photons never occupy the cavity at the same time.

#### A. Analytical solutions

Assume that the mechanical mode has been cooled to its ground state. In the weak-probe regime, only the lower energy levels of the system are excited, and the general state of the system in few-photon subspace can be written as

$$|\psi\rangle = C_{00}|00\rangle + C_{10}|10\rangle + C_{02}|02\rangle + C_{20}|20\rangle + C_{12}|12\rangle + C_{04}|04\rangle, \quad (6)$$

where the coefficients  $C_{nm}$  describe the probability amplitudes of the corresponding states. The average intracavity photon number can be expressed as

$$\langle n \rangle = |C_{10}|^2 + |C_{12}|^2 + 2|C_{20}|^2, \quad (7)$$

and the equal-time second-order correlation function

$$g^{(2)}(0) = \frac{2|C_{20}|^2}{(|C_{10}|^2 + |C_{12}|^2 + 2|C_{20}|^2)^2}. \quad (8)$$

To calculate the average intracavity photon number and the correlation function, an effective non-Hermitian Hamiltonian

is considered:

$$H'_{\text{eff}} = \Delta a^\dagger a + \tilde{\omega}_m b^\dagger b + g(a^\dagger b^2 + ab^\dagger)^2 + \varepsilon(a + a^\dagger) - i\frac{\kappa}{2}a^\dagger a - i\frac{\gamma}{2}b^\dagger b. \quad (9)$$

By the Schrödinger equation  $i\partial|\psi\rangle/dt = H'_{\text{eff}}|\psi\rangle$ , the probability amplitudes satisfy the equations of motion

$$\dot{C}_{00} = -i\varepsilon C_{10}, \quad (10a)$$

$$\dot{C}_{10} = -\kappa' C_{10} - i\sqrt{2}g C_{02} - i\varepsilon C_{00} - i\sqrt{2}\varepsilon C_{20}, \quad (10b)$$

$$\dot{C}_{02} = -2\gamma' C_{02} - i\sqrt{2}g C_{10} - i\varepsilon C_{12}, \quad (10c)$$

$$\dot{C}_{20} = -2\kappa' C_{20} - i2g C_{12} - i\sqrt{2}\varepsilon C_{10}, \quad (10d)$$

$$\dot{C}_{12} = -(\kappa' + 2\gamma') C_{12} - i2g C_{20} - i2\sqrt{3}g C_{04} - i\varepsilon C_{02}, \quad (10e)$$

$$\dot{C}_{04} = -4\gamma' C_{04} - i2\sqrt{3}g C_{12}, \quad (10f)$$

where  $\kappa' = \kappa/2 + i\Delta$ ,  $\gamma' = \gamma/2 + i\tilde{\omega}_m$ . The low mechanical decay rate  $\gamma$  ( $\ll \kappa$ ) can be neglected for simplicity, leading to  $\gamma' \approx i\tilde{\omega}_m = i\Delta/2$ . If the probe field is sufficiently weak ( $\varepsilon/\kappa \ll 1$ ), few photons will be excited to the cavity mode. In the limit  $\varepsilon \rightarrow 0$ , the system remains in the ground state  $|00\rangle$ . Thus  $C_{10}$  and  $C_{02}$  are on the scale of  $\varepsilon$ , while  $C_{20}$ ,  $C_{12}$ , and  $C_{04}$  are on the scale of  $\varepsilon^2$ .

By neglecting the higher orders of  $\varepsilon$  in the weak-probe limit, the average intracavity photon number is approximately given by  $\langle n \rangle \approx |C_{10}|^2$ . By Eq. (10) we obtain

$$\langle n \rangle = \frac{\varepsilon^2}{\kappa^2/4 + (\Delta - 2g^2/\Delta)^2} \quad (11)$$

in the case of steady state. Note that  $\langle n \rangle$  reaches the maximum value of  $4\varepsilon^2/\kappa^2$  at  $\Delta = \pm\sqrt{2}g$ . This is because the resonance transition frequency of the cavity mode from the ground state to the one-photon state is shifted by  $\pm\sqrt{2}g$  when the cavity field is coupled to the mechanical mode, as shown in Fig. 1(b).

The second-order correlation function is approximately expressed as  $g^{(2)}(0) \approx 2|C_{20}|^2/|C_{10}|^4$ . For the steady-state, we have

$$g^{(2)}(0) = \frac{[\kappa^2/4 + (\Delta - 2g^2/\Delta)^2][\kappa^2/4 + 4(\Delta - 2g^2/\Delta)^2]}{[\kappa^2/4 + \Delta^2][\kappa^2/4 + 4(\Delta - 4g^2/\Delta)^2]}. \quad (12)$$

Suppose that the probe field is tuned to the single-photon resonance transition frequency of the cavity field, i.e.,  $\Delta = \pm\sqrt{2}g$ , the correlation function becomes  $g^{(2)}(0) = 1/(1 + 8g^2/\kappa^2)(1 + 32g^2/\kappa^2)$ . In the strong-coupling regime of  $g > \kappa$ , we have  $g^{(2)}(0) < 1$ , which means that the probability of exciting the single-photon state is higher than that of preparing a two-photon state. The single-photon transition is indicated by dotted green arrows in Fig. 1(b).

In the case of two-photon resonance,  $\Delta = \pm 2g$ , the correlation function becomes  $g^{(2)}(0) = 1 + 4g^2/\kappa^2$ . We have  $g^{(2)}(0) > 1$ , which indicates that the cavity tends to be in

the two-photon state rather than the single-photon state. The two-photon transition is illustrated by the solid red arrows in Fig. 1(b).

For detuning  $\Delta = 0$ , we obtain strong photon bunching  $g^{(2)}(0) \gg 1$ . At first sight, the physical origin of this bunching seems to be the two-photon transition  $|0_0\rangle \rightarrow |2_0\rangle$ . However, the two-photon transition intermediated by two one-photon states  $|1_{\pm}\rangle$  will be suppressed as a result of destructive interference between two transition paths,  $|0_0\rangle \rightarrow |1_{-}\rangle \rightarrow |2_0\rangle$  and  $|0_0\rangle \rightarrow |1_{+}\rangle \rightarrow |2_0\rangle$ . This can be understood from the two-photon Rabi frequency  $\Omega_{0,2_0} = \sum_{k=1_{\pm}} \langle 2_0 | H'_p | k \rangle \langle k | H'_p | 2_0 \rangle / \omega_{1\pm}$ , where  $H'_p = \varepsilon(a + a^\dagger)$  is the probe field in the rotating frame and  $\omega_{1\pm} = \pm\sqrt{2}g$  are eigenvalues of the system in one-photon subspace. The two-photon Rabi frequency  $\Omega_{0,2_0}$  vanishes at zero detuning, which indicates that the two-photon resonance is annihilated by interference. In fact, as discussed for the two-mode optomechanics case [13], the photon bunching at  $\Delta = 0$  is due to the suppression of the one-photon population. Starting with the ground state  $|00\rangle$ , the system will be driven into a dark state, i.e.,  $|\text{dark}\rangle \propto g|00\rangle - \varepsilon|02\rangle$ . Hence, the population in  $|10\rangle$  is suppressed. State  $|02\rangle$  in the dark state will transit to  $|12\rangle$ , which in turn is coupled to  $|20\rangle$ .

## B. Numerical results and brief discussion

Next we solve exactly the systemic dynamics after taking into account practical noises. The master equation of the density operator  $\rho$  for the system is given by

$$\dot{\rho} = -i[H_{\text{eff}} + H_p, \rho] + \kappa\mathcal{D}[a]\rho + \gamma\bar{n}_{\text{th}}\mathcal{D}[b]\rho + \gamma(\bar{n}_{\text{th}} + 1)\mathcal{D}[b^\dagger]\rho, \quad (13)$$

where  $\mathcal{D}[o]\rho = o\rho o^\dagger - (o^\dagger o\rho + \rho o^\dagger o)/2$  is the standard dissipator in the Lindblad form and  $\bar{n}_{\text{th}} = 1/[\exp(\hbar\omega_m/k_B T) - 1]$  denotes the thermal phonon number at the environmental temperature  $T$ .

To check the validity of the effective Hamiltonian  $H_{\text{eff}}$ , the evolution of the correlation function  $g^{(2)}(0)$  is plotted in Fig. 2, where the numerical result obtained using the effective Hamiltonian  $H_{\text{eff}}$  (solid red curve) agrees well with the exact solution corresponding to the full Hamiltonian  $H_1$  (dashed blue curve). Figure 2 also shows that a steady value of the correlation function  $g^{(2)}(0)$  can be obtained at  $\kappa t \approx 20$ , which indicates that the relaxation time of the system is  $200 \mu\text{s}$  when  $\kappa = 10^5 \text{ Hz}$ .

Figure 3 plots the normalized average intracavity photon number and second-order correlation function as a function of  $\Delta/g$ . Here the average photon number is normalized by  $n_0 = 4(\varepsilon/\kappa)^2$ . The analytical results (solid red curves) are in excellent agreement with the numerical results (blue circles) based on the master equation, (13). When detuning  $\Delta = \pm\sqrt{2}g$ , Figure 3(a) shows two peaks, which are due to energy shift of the cavity field in the one-photon subspace, and Figure 3(b) presents the strong antibunching  $g^{(2)}(0) \ll 1$ , which exactly confirms the photon blockade. This effect results from the anharmonic energy level of the system. In the strong quadratic coupling regime  $g > \kappa$ , the one-photon transition  $|0_0\rangle \rightarrow |1_{\pm}\rangle$  can be spectrally resolved, and the subsequent transition  $|1_{\pm}\rangle \rightarrow |2_{0,\pm}\rangle$  is suppressed, leading to photon

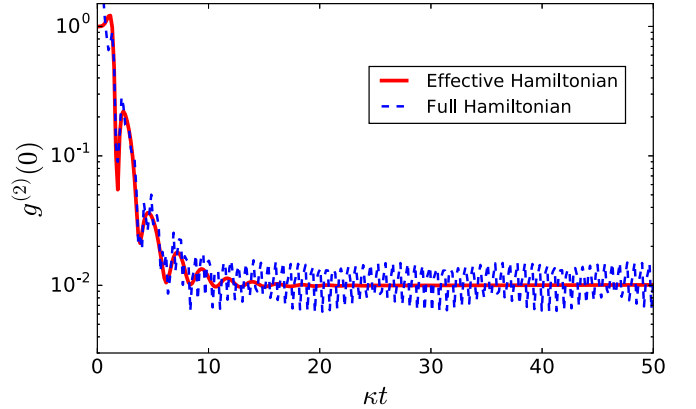


FIG. 2. Equal-time second-order correlation function  $g^{(2)}(0)$  versus  $\kappa t$  at detuning  $\Delta = \pm\sqrt{2}g$ . The solid red curve is the numerical solution based on master Eq. (13) with  $g/\kappa = 1$ ; the dashed blue curve is the exact numerical result corresponding to the full Hamiltonian  $H_1$  replacing the effective Hamiltonian  $H_{\text{eff}}$  in Eq. (13). Parameters are chosen as  $g_0/\kappa = 0.01$ ,  $\omega_m/\kappa = 100$ , and  $\alpha = 100$  (corresponding to the driving amplitude  $\Omega/\kappa \simeq 6.0 \times 10^4$ ). Other parameters are  $\bar{n}_{\text{th}} = 0$ ,  $\varepsilon/\kappa = 0.1$ , and  $\gamma/\kappa = 0.01$ .

blockade. The two peaks of  $g^{(2)}(0) > 1$  at  $\Delta = \pm 2g$  shown in Fig. 3(b) imply that the photon bunching is due to the two-photon transition  $|0_0\rangle \rightarrow |2_{\pm}\rangle$ . The two-photon transition is often referred to as photon-induced tunneling [63], where a

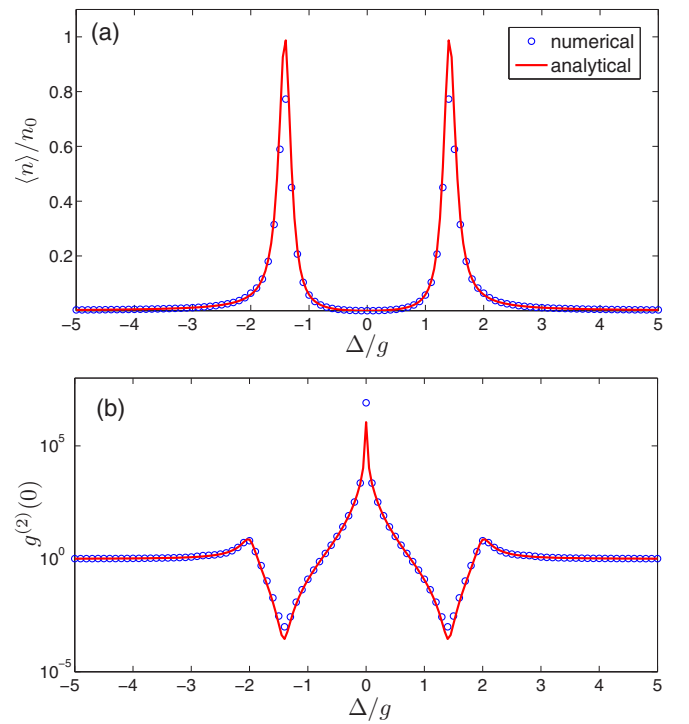


FIG. 3. (a) Normalized mean intracavity photon number  $\langle n \rangle / n_0$  with  $n_0 = 4\varepsilon^2/\kappa^2$  and (b) equal-time second-order correlation function  $g^{(2)}(0)$  as a function of  $\Delta/g$  at zero temperature. Solid red curves show approximate analytical results based on Eqs. (11) and (12); blue circles show numerical solutions of the master equation. Parameters are taken as  $g/\kappa = 4$ ,  $\varepsilon/\kappa = 0.1$ , and  $\gamma/\kappa = 0.01$ .

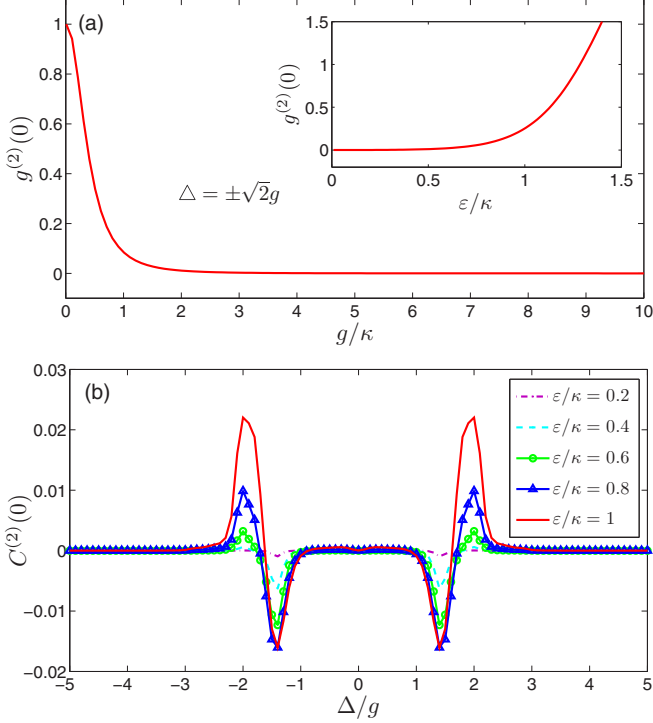


FIG. 4. (a) At detuning  $\Delta = \pm\sqrt{2}g$ , the second-order correlation function  $g^{(2)}(0)$  as a function of  $g/\kappa$  with  $\varepsilon/\kappa = 0.1$ . Inset:  $g^{(2)}(0)$  as a function of  $\varepsilon/\kappa$ . (b) Second-order differential correlation function  $C^{(2)}(0)$  versus  $\Delta/g$  for different values of  $\varepsilon/\kappa$ . Other parameters are  $\gamma/\kappa = 0.01$  and  $g/\kappa = 4$ .

photon presenting into the cavity will increase the probability of a subsequent photon's entering it. The bunching effect at  $\Delta = 0$  results from the suppression of the one-photon state, as discussed in the previous subsection.

Figure 4(a) displays the correlation function  $g^{(2)}(0)$  as a function of  $g/\kappa$  at the detuning  $\Delta = \pm\sqrt{2}g$ . Obviously,  $g^{(2)}(0)$  decreases with increasing  $g/\kappa$ , and  $g^{(2)}(0) \ll 1$  appears in the region  $g/\kappa > 1$ , which implies that the strong-coupling condition is necessary for generating photon blockade. The inset describes  $g^{(2)}(0)$  for different values of  $\varepsilon/\kappa$ , where the coupling strength  $g = \kappa$ . We find that  $g^{(2)}(0) \ll 1$  can be observed only in the weak-probe limit  $\varepsilon/\kappa \ll 1$ , and  $g^{(2)}(0)$  increases with increasing  $\varepsilon/\kappa$ . The photon antibunching disappears when the probe amplitude  $\varepsilon$  exceeds the cavity decay rate  $\kappa$ .

The photon-induced tunneling can be better measured by the second-order differential correlation function [66,67]  $C^{(2)}(0) = \langle a^{\dagger 2} a^2 \rangle - \langle a^{\dagger} a \rangle^2 = [g^{(2)}(0) - 1]\langle n \rangle^2$ , which characterizes the probability of generating simultaneously two photons in the cavity.  $C^{(2)}(0) > 0$  denotes the photon-induced tunneling effect. Figure 4(b) shows  $C^{(2)}(0)$  as a function of  $\Delta/g$ . Two peaks arise at  $\Delta = \pm 2g$ , and  $C^{(2)}(0)$  increases with increasing  $\varepsilon/\kappa$ . This means that the weak-probe limit is not required for photon tunneling, which is different from photon blockade at  $\Delta = \pm\sqrt{2}g$ .

Since both one-photon and two-photon transitions depend on the phonon state  $|m\rangle$ , the thermal noise of the mechanical environment will degrade the quality of photon blockade and

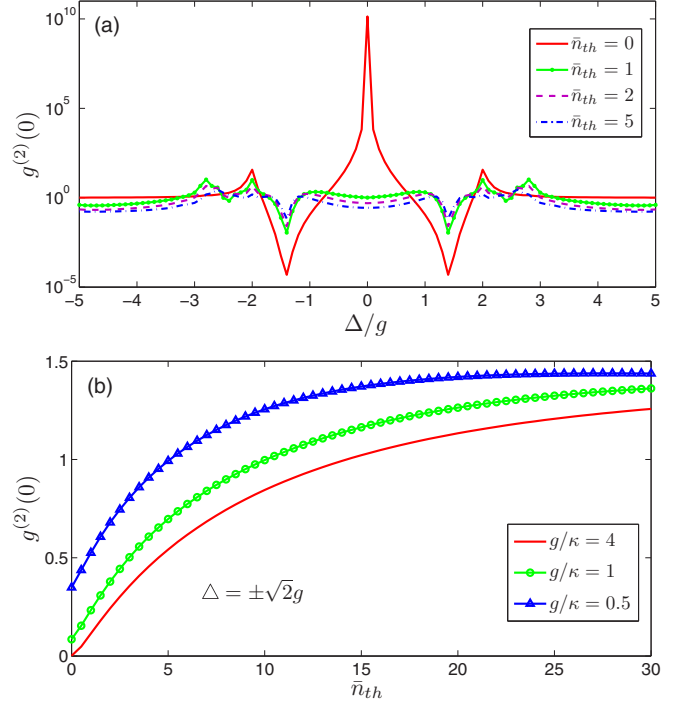


FIG. 5. (a) Second-order correlation function  $g^{(2)}(0)$  versus  $\Delta/g$  for various thermal phonon occupancy  $\bar{n}_{th}$ . Parameters are selected as  $\varepsilon/\kappa = 0.1$ ,  $\gamma/\kappa = 0.001$ , and  $g/\kappa = 10$ . (b) Second-order correlation function  $g^{(2)}(0)$  versus  $\bar{n}_{th}$  at  $\Delta = \pm\sqrt{2}g$  for different coupling strengths  $g/\kappa$ . Parameters are chosen as  $\varepsilon/\kappa = 0.1$  and  $\gamma/\kappa = 0.01$ .

photon-induced tunneling. The correlation function  $g^{(2)}(0)$  as a function of  $\Delta/g$  for different thermal phonon occupations  $\bar{n}_{th}$  is displayed in Fig. 5(a). It is noteworthy that, in the strong-coupling regime, the feature of the one-photon transition remains in the presence of a small but finite thermal phonon number. Figure 5(a) also exhibits several interesting features of the correlation function  $g^{(2)}(0)$  for small thermal occupation. First, at detuning  $\Delta = 0$ , the photon bunching quickly converts to antibunching when the thermal phonon number increases. Second, except for the two-photon resonance at  $\Delta = \pm 2g$ , several new resonances emerge in the correlation function. In addition, in the case of zero temperature ( $\bar{n}_{th} = 0$ ), there is neither bunching nor antibunching at the large detuning  $\Delta > 2g$ , but at finite temperature new bunching and antibunching effects appear. To understand these new features, we assume that the mechanical mode is initially in a thermal state at temperature  $T$  and the cavity in the vacuum state. The system can be depicted by the density matrix  $\rho = (1 - p) \sum_{m \geq 0} p^m |0m\rangle \langle 0m|$ , where  $p = \exp(-\hbar\omega_m/k_B T)$ . In this case, the splitting of the dressed energy level is  $m$  dependent, so that the individual resonances within each  $m$  subspace may be overlapped. The cumulative effect of different phonon numbers leads to new resonances and antibunching features [10–12]. Figure 5(b) presents  $g^{(2)}(0)$  as a function of  $\bar{n}_{th}$  at  $\Delta = \pm\sqrt{2}g$ . The photon antibunching [ $g^{(2)}(0) < 1$ ] still survives in the weak-coupling regime even with a finite thermal phonon number. This result differs from an early study [58] of photon blockade, in which the photon antibunching disappears for small thermal phonon numbers even in the strong-coupling limit.

#### IV. EXPERIMENTAL PROSPECTS AND CONCLUSIONS

To generate photon blockade and photon-induced tunneling, the condition  $\omega_m \gg g > \kappa \gg \gamma$  must be satisfied. Currently, some optomechanical systems have already demonstrated a high mechanical frequency and low-loss optical mode [54,55], so that the condition  $\omega_m \gg \kappa \gg \gamma$  is met. The key challenge is the strong-coupling condition  $g > \kappa$ . Fortunately, the single-photon quadratic coupling strength  $g_0$  has been greatly enhanced, to 245 Hz, in the photonic crystal optomechanical cavity [65], so that the strong-coupling condition  $g > \kappa$  is possible for  $\alpha \sim 10^4$  [55]. Although the cavity decay rate and mechanical frequency in Ref. [65] operate outside the sideband-resolved regime ( $\kappa = 5$  GHz and  $\omega_m = 10$  MHz), it has been shown that a low-loss optical mode  $\kappa = 20$  MHz can be obtained in a similar planar silicon photonic crystal [68], and a higher mechanical frequency,  $\omega_m = 225$  MHz, can be employed with some high-order modes of the central nanobeam. Therefore, our proposal could be implemented with currently available optomechanical technology.

In summary, we have studied photon blockade and photon-induced tunneling in a strongly driven optomechanical system with quadratic coupling. By driving the cavity on

red two-phonon resonance, the effective nonlinear coupling between photons and phonons can be enhanced and tuned via adjustment of the driving amplitude. We have obtained an approximate analytical solution as well as a numerical simulation result for the second-order correlation function and have found that the photon blockade at detuning  $\Delta = \pm\sqrt{2}g$  and photon-induced tunneling at detuning  $\Delta = \pm 2g$  can be realized in the strong-coupling regime  $g > \kappa$ . Our results provide a possible route for realization of single-photon nonlinearities and for applications of optomechanical systems in quantum information processing.

#### ACKNOWLEDGMENTS

We thank Jiang-Min Zhang and Ming-Yong Ye for valuable suggestions regarding the manuscript. We also acknowledge support from the National Natural Science Foundation of China (Grants No. 61275215, No. 61308012, and No. 11202080), the National Fundamental Research Program of China (Grant No. 2011CBA00203), the Natural Science Foundation of Fujian Province of China (Grants No. 2016J01009 and No. 2013J01008), and the Educational Department Project of Fujian Province of China (Grant No. JA14075).

- 
- [1] A. Imamoğlu, H. Schmidt, G. Woods, and M. Deutsch, *Phys. Rev. Lett.* **79**, 1467 (1997).
  - [2] K. M. Birnbaum, A. Boca, R. Miller, A. D. Boozer, T. E. Northup, and H. J. Kimble, *Nature* **436**, 87 (2005).
  - [3] A. Reinhard, T. Volz, M. Winger, A. Badolato, K. J. Hennessy, E. L. Hu, and A. Imamoğlu, *Nat. Photon.* **6**, 93 (2012).
  - [4] H. Gorniaczyk, C. Tresp, J. Schmidt, H. Fedder, and S. Hofferberth, *Phys. Rev. Lett.* **113**, 053601 (2014).
  - [5] S. Baur, D. Tiarks, G. Rempe, and S. Dürr, *Phys. Rev. Lett.* **112**, 073901 (2014).
  - [6] T. J. Kippenberg and K. J. Vahala, *Science* **321**, 1172 (2008).
  - [7] M. Aspelmeyer, T. J. Kippenberg, and F. Marquardt, *Rev. Mod. Phys.* **86**, 1391 (2014).
  - [8] S. Bose, K. Jacobs, and P. Knight, *Phys. Rev. A* **56**, 4175 (1997).
  - [9] C. Fabre, M. Pinard, S. Bourzeix, A. Heidmann, E. Giacobino, and S. Reynaud, *Phys. Rev. A* **49**, 1337 (1994).
  - [10] A. Nunnenkamp, K. Børkje, and S. M. Girvin, *Phys. Rev. Lett.* **107**, 063602 (2011).
  - [11] P. Rabl, *Phys. Rev. Lett.* **107**, 063601 (2011).
  - [12] K. Stannigel, P. Komar, S. J. M. Habraken, S. D. Bennett, M. D. Lukin, P. Zoller, and P. Rabl, *Phys. Rev. Lett.* **109**, 013603 (2012).
  - [13] P. Komar, S. D. Bennett, K. Stannigel, S. J. M. Habraken, P. Rabl, P. Zoller, and M. D. Lukin, *Phys. Rev. A* **87**, 013839 (2013).
  - [14] J. Qian, A. A. Clerk, K. Hammerer, and F. Marquardt, *Phys. Rev. Lett.* **109**, 253601 (2012).
  - [15] J.-Q. Liao, H. K. Cheung, and C. K. Law, *Phys. Rev. A* **85**, 025803 (2012).
  - [16] J.-Q. Liao and C. K. Law, *Phys. Rev. A* **87**, 043809 (2013).
  - [17] A. Kronwald, M. Ludwig, and F. Marquardt, *Phys. Rev. A* **87**, 013847 (2013).
  - [18] M.-A. Lemonde, N. Didier, and A. A. Clerk, *Phys. Rev. Lett.* **111**, 053602 (2013).
  - [19] K. Børkje, A. Nunnenkamp, J. D. Teufel, and S. M. Girvin, *Phys. Rev. Lett.* **111**, 053603 (2013).
  - [20] Y.-C. Liu, Y.-F. Xiao, Y.-L. Chen, X.-C. Yu, and Q. Gong, *Phys. Rev. Lett.* **111**, 083601 (2013).
  - [21] A. Kronwald and F. Marquardt, *Phys. Rev. Lett.* **111**, 133601 (2013).
  - [22] X.-Y. Lü, Y. Wu, J. R. Johansson, H. Jing, J. Zhang, and F. Nori, *Phys. Rev. Lett.* **114**, 093602 (2015).
  - [23] M. Ludwig, A. H. Safavi-Naeini, O. Painter, and F. Marquardt, *Phys. Rev. Lett.* **109**, 063601 (2012).
  - [24] A. A. Clerk, F. Marquardt, and J. G. E. Harris, *Phys. Rev. Lett.* **104**, 213603 (2010).
  - [25] H. Miao, S. Danilishin, T. Corbitt, and Y. Chen, *Phys. Rev. Lett.* **103**, 100402 (2009).
  - [26] F. Marquardt, J. P. Chen, A. A. Clerk, and S. M. Girvin, *Phys. Rev. Lett.* **99**, 093902 (2007).
  - [27] I. Wilson-Rae, N. Nooshi, W. Zwerger, and T. J. Kippenberg, *Phys. Rev. Lett.* **99**, 093901 (2007).
  - [28] A. Schliesser, R. Rivière, G. Anetsberger, O. Arcizet, and T. J. Kippenberg, *Nat. Phys.* **4**, 415 (2008).
  - [29] T. Rocheleau, T. Ndukum, C. Macklin, J. Hertzberg, A. Clerk, and K. Schwab, *Nature* **463**, 72 (2010).
  - [30] A. D. O'Connell *et al.*, *Nature* **464**, 697 (2010).
  - [31] J. Teufel, T. Donner, D. Li, J. Harlow, M. Allman, K. Cicak, A. Sirois, J. D. Whittaker, K. Lehnert, and R. W. Simmonds, *Nature* **475**, 359 (2011).
  - [32] J. Chan, T. M. Alegre, A. H. Safavi-Naeini, J. T. Hill, A. Krause, S. Gröblacher, M. Aspelmeyer, and O. Painter, *Nature* **478**, 89 (2011).
  - [33] S. Gröblacher, K. Hammerer, M. R. Vanner, and M. Aspelmeyer, *Nature* **460**, 724 (2009).

- [34] J. Teufel, D. Li, M. Allman, K. Cicak, A. Sirois, J. Whittaker, and R. Simmonds, *Nature* **471**, 204 (2011).
- [35] G. S. Agarwal and S. Huang, *Phys. Rev. A* **81**, 041803 (2010).
- [36] S. Weis, R. Rivière, S. Deléglise, E. Gavartin, O. Arcizet, A. Schliesser, and T. J. Kippenberg, *Science* **330**, 1520 (2010).
- [37] A. H. Safavi-Naeini, T. M. Alegre, J. Chan, M. Eichenfield, M. Winger, Q. Lin, J. T. Hill, D. E. Chang, and O. Painter, *Nature* **472**, 69 (2011).
- [38] V. Fiore, Y. Yang, M. C. Kuzyk, R. Barbour, L. Tian, and H. Wang, *Phys. Rev. Lett.* **107**, 133601 (2011).
- [39] Y.-D. Wang and A. A. Clerk, *Phys. Rev. Lett.* **108**, 153603 (2012).
- [40] L. Tian, *Phys. Rev. Lett.* **108**, 153604 (2012).
- [41] C. Dong, V. Fiore, M. C. Kuzyk, and H. Wang, *Science* **338**, 1609 (2012).
- [42] T. Palomaki, J. Harlow, J. Teufel, R. Simmonds, and K. Lehnert, *Nature* **495**, 210 (2013).
- [43] J. T. Hill, A. H. Safavi-Naeini, J. Chan, and O. Painter, *Nat. Commun.* **3**, 1196 (2012).
- [44] D. W. Brooks, T. Botter, S. Schreppler, T. P. Purdy, N. Brahms, and D. M. Stamper-Kurn, *Nature* **488**, 476 (2012).
- [45] A. H. Safavi-Naeini, S. Gröblacher, J. T. Hill, J. Chan, M. Aspelmeyer, and O. Painter, *Nature* **500**, 185 (2013).
- [46] T. P. Purdy, P.-L. Yu, R. W. Peterson, N. S. Kampel, and C. A. Regal, *Phys. Rev. X* **3**, 031012 (2013).
- [47] T. T. Heikkilä, F. Massel, J. Tuorila, R. Khan, and M. A. Sillanpää, *Phys. Rev. Lett.* **112**, 203603 (2014).
- [48] A. Xuereb, C. Genes, and A. Dantan, *Phys. Rev. Lett.* **109**, 223601 (2012).
- [49] A. Xuereb, C. Genes, and A. Dantan, *Phys. Rev. A* **88**, 053803 (2013).
- [50] G. Via, G. Kirchmair, and O. Romero-Isart, *Phys. Rev. Lett.* **114**, 143602 (2015).
- [51] X.-Y. Lü, W.-M. Zhang, S. Ashhab, Y. Wu, and F. Nori, *Sci. Rep.* **3**, 2943 (2013).
- [52] X. Xu, M. Gullans, and J. M. Taylor, *Phys. Rev. A* **91**, 013818 (2015).
- [53] A. Jayich, J. Sankey, B. Zwickl, C. Yang, J. Thompson, S. Girvin, A. Clerk, F. Marquardt, and J. Harris, *New J. Phys.* **10**, 095008 (2008).
- [54] J. Thompson, B. Zwickl, A. Jayich, F. Marquardt, S. Girvin, and J. Harris, *Nature* **452**, 72 (2008).
- [55] J. C. Sankey, C. Yang, B. M. Zwickl, A. M. Jayich, and J. G. Harris, *Nat. Phys.* **6**, 707 (2010).
- [56] T. P. Purdy, D. W. C. Brooks, T. Botter, N. Brahms, Z.-Y. Ma, and D. M. Stamper-Kurn, *Phys. Rev. Lett.* **105**, 133602 (2010).
- [57] D. J. Wilson, C. A. Regal, S. B. Papp, and H. J. Kimble, *Phys. Rev. Lett.* **103**, 207204 (2009).
- [58] J.-Q. Liao and F. Nori, *Phys. Rev. A* **88**, 023853 (2013).
- [59] A. Nunnenkamp, K. Børkje, J. G. E. Harris, and S. M. Girvin, *Phys. Rev. A* **82**, 021806 (2010).
- [60] M. Asjad, G. S. Agarwal, M. S. Kim, P. Tombesi, G. Di Giuseppe, and D. Vitali, *Phys. Rev. A* **89**, 023849 (2014).
- [61] H. Tan, G. Li, and P. Meystre, *Phys. Rev. A* **87**, 033829 (2013).
- [62] H. Shi and M. Bhattacharya, *Phys. Rev. A* **87**, 043829 (2013).
- [63] A. Faraon, I. Fushman, D. Englund, N. Stoltz, P. Petroff, and J. Vučković, *Nat. Phys.* **4**, 859 (2008).
- [64] C. Lang, D. Bozyigit, C. Eichler, L. Steffen, J. M. Fink, A. A. Abdumalikov, M. Baur, S. Filipp, M. P. da Silva, A. Blais, and A. Wallraff, *Phys. Rev. Lett.* **106**, 243601 (2011).
- [65] T. K. Paraïso, M. Kalae, L. Zang, H. Pfeifer, F. Marquardt, and O. Painter, *Phys. Rev. X* **5**, 041024 (2015).
- [66] A. Kubanek, A. Ourjoumtsev, I. Schuster, M. Koch, P. W. H. Pinkse, K. Murr, and G. Rempe, *Phys. Rev. Lett.* **101**, 203602 (2008).
- [67] X.-W. Xu, Y.-J. Li, and Y.-X. Liu, *Phys. Rev. A* **87**, 025803 (2013).
- [68] H. Sekoguchi, Y. Takahashi, T. Asano, and S. Noda, *Opt. Express* **22**, 916 (2014).